SCIENCE CHINA Materials ARTICLES

mater.scichina.com link.springer.com

Published online 12 June 2019 | https://doi.org/10.1007/s40843-019-9442-x
Sci China Mater 2019, 62(10): 1385–1392

Hierarchical flower-like spinel manganese-based oxide nanosheets for high-performance lithium ion battery

Quanqing Zhao[1], Zefeng Guo[2], Yu Wu[1], Liqin Wang[1], Zhanli Han[1], Xilan Ma[1], Youqi Zhu[1] and Chuanbao Cao[1*]

ABSTRACT **Hierarchical flower-structured two-dimensional (2D) nanosheet is favorable for electrochemical reactions. The unique structure not only exposes the maximized active sites and shortens ion/electron diffusion channels, but also inhibits the structural strain during cycling processes. Herein, we report the hierarchical flower-like pure spinel manganese-based oxide nanosheets synthesized *via* a template-orientated strategy. The oriented template is fabricated by decomposition of carbonate obtained from "bubble reaction" *via* an alcohol-assisted hydrothermal process. The resultant spinel manganese-based oxide nanosheets simultaneously possess excellent rate capability and cycling stability. The high-voltage $LiNi_{0.5}Mn_{1.5}O_4$ (LNMO-HF) has a uniform phase distribution without the common impurity phase $Li_xNi_{1-x}O_2$ and Ni_xO. Besides, the LNMO-HF delivers high discharge capacity of 142.6 mA h g^{-1} with specific energy density of 660.7 W h kg^{-1} at 1 C under 55°C. More importantly, the template-orientated strategy can be extended to the synthesis of $LiMn_2O_4$ (LMO), which can achieve 88.12% capacity retention after 1000 cycles.**

Keywords: nanosheet, flower-like structure, manganese-based oxide, lithium ion battery

INTRODUCTION

In view of the ever-increasing demand for high energy density, especially for power electric vehicles (EVs) and hybrid EVs, the development of the high voltage and high capacity cathode materials for next-generation lithium ion batteries is highly desired but still remains a challenge [1–3]. Spinel manganese-based oxide has attracted extensive attention owing to its high theoretical specific capacity and fast three-dimensional lithium ion diffusion channel. Especially, high-voltage $LiNi_{0.5}Mn_{1.5}O_4$ (LNMO-HF) has shown huge potential on account of a high and stable voltage platform of ~4.7 V [4–9]. Furthermore, spinel $LiNi_{0.5}Mn_{1.5}O_4$ possesses excellent high specific energy density which is beyond that of the commercial $LiCoO_2$ and $LiFePO_4$ [10–12]. However, bulk spinel manganese-based oxide cathodes are generally subject to capacity and rate capability degradation due to sensitive factors induced during synthesis, namely Mn^{3+} ions produced by oxygen deficiency and impurity phase $Li_xNi_{1-x}O_2$ and Ni_xO. Among them, Mn^{2+} produced by the decomposition of Mn^{3+} is dissolved in the electrolyte to cause collapse of the spinel manganese-based cathode structure at elevated temperatures. In addition, the impurity phases can also accelerate the structural deterioration resulting in a low capacity. Compared with bulk material, the hierarchical nanostructured material is beneficial to alleviating these disadvantages [9,11].

Novel nanostructured (zero-dimensional (0D), 1D, 2D) materials can impart excellent physical and chemical properties compared to the corresponding bulk material in various energy fields [13–15]. Among them, 2D (nanoplates, nanosheets) materials have shown remarkable attraction deriving from their 2D ion transport channels as well as high surface area [16–18]. It is well-known that 2D electrode materials for lithium ion betteries contribute to high capacity, long cycle life and superior rate performance by increasing the contact area of the electrode/electrolyte, exposing a large number of active sites, as well as facilitating electron/Li^+ ions diffusion channel [19–21]. Enormous efforts about 2D electrode materials have been devoted to the anode electrode, such as SnSe [22], Co_3O_4

[1] Research Center of Materials Science, Beijing Key Laboratory of Construction Tailorable Advanced Functional Materials and Green Applications, Beijing Institute of Technology, Beijing 100081, China
[2] Datong Coal Mine Group Shuozhou Coal Co. Ltd, Huairen 038300, China
* Corresponding author (email: cbcao@bit.edu.cn)

 © Science China Press and Springer-Verlag GmbH Germany, part of Springer Nature 2019

[20], graphene [23], and so on. In comparison, reports on 2D cathode materials are very few, most of which are dedicated to the synthesis of $LMPO_4$ [14,24,25]. Metal oxide cathode materials are usually accompanied by conventional high temperature calcination during the lithiation process. Phase transformation and crystal growth can bring about the destruction of 2D structures in this process [26–30]. Therefore, developing appropriate synthetic methods for 2D oxide cathode materials is urgent.

The hierarchical architectures constructed from nanostructure with specific dimensions have attracted extensive interest because of their intriguing properties and various potential applications [31–36]. A 3D architecture assembled by nanostructure simultaneously combines the advantages of nanostructures and microstructures. Based on the advantages of the aforementioned 2D structure for lithium ion battery, hierarchical architectures not only lead to larger specific surface area and shorten the electron/Li^+ transfer distance, but also could sustain their structure during the repeated cycles [31–35]. Meanwhile, porous structure effectively facilitates the penetration of electrolyte [35,37]. Currently, the construction of hierarchical architectures combined with 2D structure remains a great challenge for spinel manganese-based cathode.

Herein, the hierarchical flower-like pure spinel manganese-based oxide nanosheets synthesized *via* a template-orientated strategy as high-performance cathode are reported. The orientated transition metal oxide (TMO) precursors can facilitate the infiltration of the lithium source and weaken the collapse of the structure caused by the phase change during lithiation, maintaining the 2D nanosheet structure. In addition, the resultant hierarchical flower-like spinel manganese-based cathode simultaneously possesses excellent rate capacity and high cycling stability. The as-synthesized high-voltage LNMO-HF can present an initial capacity of 138.5 mA h g^{-1} at 1 C and achieve high capacity retentions of 94.2% at 5 C and 86.5% at 10 C. Furthermore, LNMO-HF can also deliver high discharge capacity of 142.6 mA h g^{-1} with specific energy density of 660.7 W h kg^{-1} at 1 C under 55°C. More importantly, the template-orientated strategy can be extended to the synthesis of $LiMn_2O_4$ (LMO), which can retain 88.12% capacity retention after 1000 cycles.

EXPERIMENTAL SECTION

Preparation of materials

The flower-like TMO precursor microspheres self-assembled from nanosheets were synthesized by the hydrothermal process and consequent thermal treatment. Typically, for the LNMO-HF precursors, hexamethylenetetramine (HMT) and corresponding stoichiometric ratio of $Mn(Ac)_2{\cdot}4H_2O$ and $Ni(Ac)_2{\cdot}4H_2O$ were successively dissolved in a certain amount of deionized water under stirring at room temperature. The ethanol solution (the volume ratio of water to ethanol 5:2) was added to the above solution and stirred for 2 h. Then the mixture solution was poured into the stainless steel vessel and heated at 150°C for 24 h. After being repeatedly washed with deionized water and ethanol, the obtained precipitation was converted to TMO precursors *via* heating at 400°C for 8 h. The LMO precursors were prepared with the same procedure using $Mn(Ac)_2{\cdot}4H_2O$ and isopropanol solution (the volume ratio of water to isopropanol 5:2). Then, TMO and $LiOH{\cdot}H_2O$ with stoichiometric ratio were dispersed in a small amount of ethanol to form suspension, and after drying overnight, the compound was grounded and sintered at 750°C for 6 h to obtain LNMO-HF and 700°C for 8 h to obtain LMO, respectively.

Additional experiment

The other way to synthesize LNMO was sol-gel method. Typically, the corresponding stoichiometric ratio of metal acetate ($Li(Ac){\cdot}2H_2O$, $Mn(Ac)_2{\cdot}4H_2O$ and $Ni(Ac)_2{\cdot}4H_2O$) were added to an aqueous solution of citric acid with stirring at 80°C, where the molar ratio of citric acid to transition metal acetate was 2:1. Then ammonia water was added to the above solution to adjust the pH to ~8. Then the obtained solution was completely evaporated under stirring at 80°C to get dry gel. The as-obtained materials were preheated at 400°C for 8 h and sintered at 750°C for 6 h to get LNMO (LNMO-SG).

Characterization

The phase structure of samples was analyzed by the X-ray diffraction (XRD) (PANalytical X-pert diffractometer, Netherlands) with Cu-Kα radiation from 10° to 80°. The element contents of the samples were examined by inductively coupled plasma atomic emission spectrometry (ICP-AES, ICAP-6300). X-ray photoelectron spectroscopy (XPS, PHI Quanteral II, Japan) was applied to determine the surface element composition of LNMO. A Hitachi field-emission scanning electron microscope (FESEMS, Hitachi S-4800) and transmission electron microscope (TEM) (HRTEM, FEI Tecnai G2 F20, 200 kV) were conducted to further observe the morphology and crystal structure of the precursors and spinel

 © Science China Press and Springer-Verlag GmbH Germany, part of Springer Nature 2019

manganese-based cathode.

The electrochemical tests were performed by CR2025 coin-shaped half-cells assembled in an Ar-filled glove box. The cathode slurry was prepared by mixing active material, acetylene black, and polyvinylidene fluoride in *N*-methyl-2-pyrrolidone with the mass ratio of 7:2:1, which was coated on the aluminum foil. The mass loading of active materials on the electrode was about 1.5 mg cm^{-2}. The electrolyte of high-voltage phase was 1 mol L^{-1} $LiPF_6$ dissolved in ethyl carbonate-dimethyl carbonate (EC-DMC, 3:7 *v*/*v*). The electrolyte of LMO was 1 mol L^{-1} $LiPF_6$ dissolved in ethyl carbonate-dimethyl carbonate (EC-DMC, 1:1 *v*/*v*). Galvanostatic charge-discharge tests were conducted on CT2001A Land battery testing system. Cyclic voltammetry (CV) was measured on IM6e electrochemical workstation (Zahner, Germany) at a scan rate of 0.1 mV s^{-1}.

RESULTS AND DISCUSSION

Fig. 1 illustrates the procedure for preparation of the hierarchical spinel manganese-based oxide nanosheets. The hydrothermal synthesis mechanism of transition metal carbonate is similar to previous report [30]. A kind of "bubble reaction" with alcohol-assisted hydrothermal process was introduced. The abundant CO_2 bubbles generated by the decomposition of HMT combined with the transition metal ions to form carbonate precipitates when the solvothermal temperature exceeded 130°C. Subsequently, the obtained carbonates were converted to TMO precursors by pre-calcination with the release of CO_2. Finally, Li was implanted into TMO precursors by high temperature sintering, resulting in hierarchical flower-like spinel manganese-based cathode nanosheets.

The structure and morphology of the as-synthesized transition metal carbonate precursors were analyzed by XRD patterns and SEM (Supplementary information, Figs S1 and S2a, b). The SEM images of LNMO-HF precursors are presented in Fig. 2a, b. After the thermodynamic decomposition of carbonate precursor, TMO

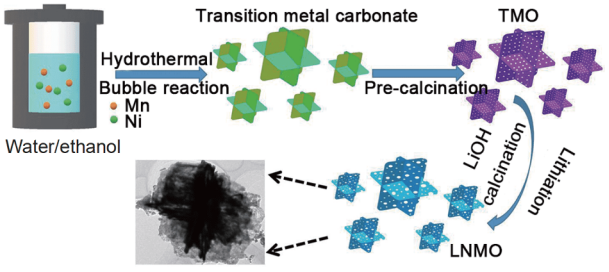

Figure 1 Schematic illustration of the formation of LNMO-HF.

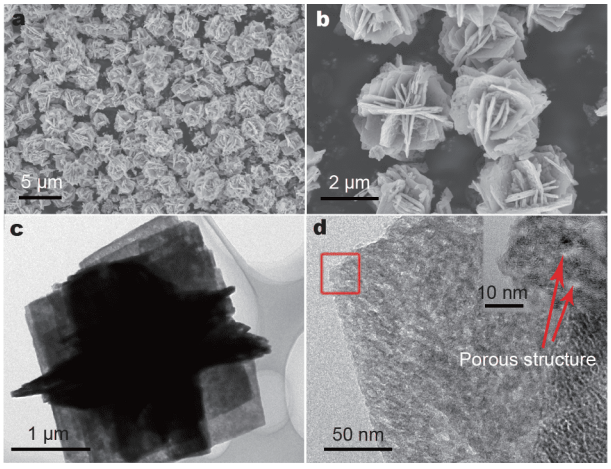

Figure 2 SEM (a, b) and TEM (c, d) images of TMO precursors.

precursors with uniform size flower-like microspheres self-assembled from 2D nanosheets inherit the morphology of carbonate. The ICP indicates that the ratio of Mn/Ni in TMO is about 3.03, corresponding to the theoretically calculated value. The thickness of nanosheets is about 50 nm. As shown in Fig. 2c, d, TEM images of TMO further confirm the results of SEM. From the high magnification image, plenty of pores are in the nanosheets owing to the release of CO_2 during decomposition of carbonate precursors, which is beneficial to the infiltration of Li and the formation of the final product LNMO-HF.

In Fig. 3a, the XRD pattern of the as-synthesized LNMO-HF shows sharp diffraction peaks demonstrating high crystallinity. All the diffraction peaks are indexed and consistent with spinel phase $LiNi_{0.5}Mn_{1.5}O_4$ (JCPDS #80-2162) [9]. It is worth noting that the common impurity phase $Li_xNi_{1-x}O_2$ [6,9] for LNMO-HF is hardly observed in the pattern. That may be attributed to the hydrothermal synthesis method and the structure of the precursor, which shorten the time of solid phase reaction during lithiation and inhibit the formation of impurity phase. The elements on the surface of LNMO-HF were analyzed by XPS. Fig. 3b shows the full-scale spectrum of the relevant elements on the surface. As shown in Fig. 3c, the Mn 2p is deconvoluted into Mn^{3+}–O bond and Mn^{4+}–O to determine the valence distribution of Mn [38]. It can be seen that the content ratio of Mn^{3+}/Mn^{4+} on the surface of LNMO-HF is about 59%, less than that of LNMO-SG (78%) in Fig. S3c, corresponding to the charge/discharge voltage plots at around 4 V (Fig. S4). Combined with the XPS results of LNMO-SG and Mn 2p from the separator surface (Fig. S5), it can be concluded

 © Science China Press and Springer-Verlag GmbH Germany, part of Springer Nature 2019

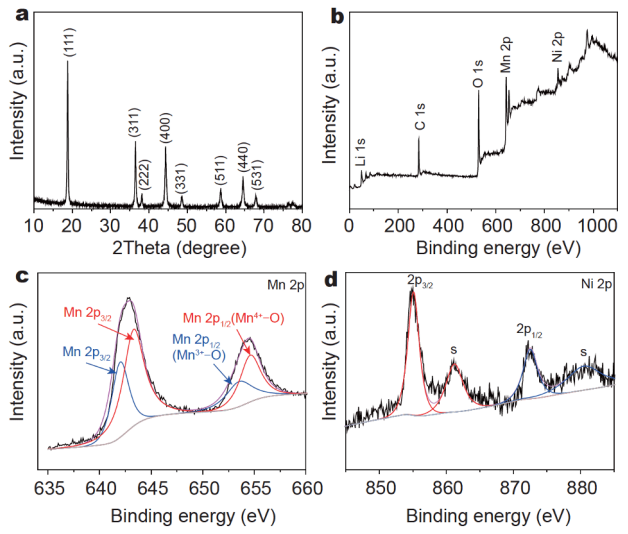

Figure 3 XRD pattern of the LNMO-HF (a). The full-scale (b), Mn 2p (c) and Ni 2p (d) XPS curves of LNMO-HF.

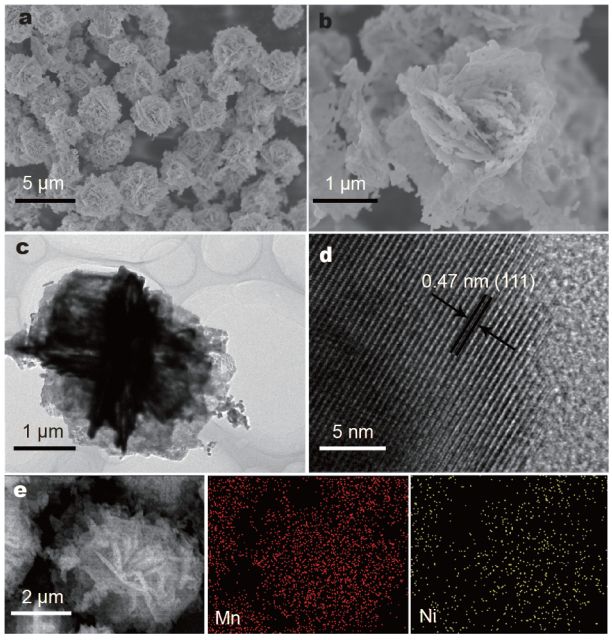

Figure 4 SEM (a and b), TEM (c) and HRTEM (d) images, SEM images and element mapping (e) of LNMO-HF.

that the appropriate amount of Mn^{3+} can reduce Jahn-Teller effect and increase ionic conductivity for the fast Li^+ diffusion [6,10]. However, trace amount of Mn cations is detected in electrolyte according to ICP result with 2 wt% dissolved Mn compared with the original Mn content. Therefore, it is still a great challenge to completely inhibit Jahn-Teller effect. In addition, the main peak and satellite peak of Ni 2p at Ni $2p_{1/2}$ and Ni $2p_{3/2}$ can be easily distinguished in Fig. 3d, where the satellite peak is mainly attributed to multiple splitting of the energy levels in nickel oxide (NiO) [10,38], demonstrating the coexistence of +2 and +3 Ni.

The morphology of the spinel manganese-based oxide cathode material was investigated by SEM, as shown in Fig. 4. The SEM images of LNMO-HF show the unique hierarchical flower-like structure self-assembled by 2D nanosheets even after high temperature lithiation. In Fig. 4b, each nanosheet is assembled from a myriad of nanoparticles, exhibiting a multi-hole structure. SEM image of similar structure LMO is shown in Fig. S2d. Furthermore, the microstructure of the as-prepared LNMO-HF was further analyzed by TEM. As shown in Fig. 4c, the LNMO-HF does inherit the morphology of the TMO precursor. The unique morphology not only maximizes the active sites to promote Li^+ diffusion, but also ensures good structural stability to inhibit the structural strains during repeated cycling process. As shown in Fig. 4d, the HRTEM image of a single LNMO-HF nanosheet illustrates the measured lattice spacing of 0.47 nm, well corresponding to the (111) planes of LNMO-HF. In addition, the Ni and Mn uniformly distribute in the element mapping of LNMO-HF in Fig. 4e.

The electrochemical performances of the final spinel manganese-based oxide nanosheets cathode were evaluated by galvanostatic charge/discharge measurement. As shown in Fig. 5a, the cycle performances of LNMO-HF cathode were carried out at 1 C under room temperature. The initial discharge capacity of LNMO-HF is 136 mA h g^{-1} with capacity retention rate of 92.7% up to 100 cycles, corresponding to Coulombic efficiency of almost 100%. In contrast, the LNMO-SG yields the initial discharge capacity of 126.3 mA h g^{-1} and capacity retention rate of 71.49%. In addition, taking the demand of high energy density for EVs into consideration, the evaluation of rate performance is also essential. The as-prepared samples were charged-discharged at various rates in Fig. 5b. The LNMO-HF exhibits excellent rate performance. When the current density was switched to 1 C again, the discharge capacity of LNMO-HF can recover the initial discharge capacity. Impressively, compared with the initial capacity of 138.5 mA h g^{-1} obtained at 1 C, the capacity retention of around 94.2% and 86.5% at 5 and 10 C, respectively can be achieved for LNMO-HF. Meanwhile, these results are higher than most of the LNMO reported previously (Table S1).

Fig. 5c displays the specific energy density of the LNMO-HF cathode at various discharge current den-

 © Science China Press and Springer-Verlag GmbH Germany, part of Springer Nature 2019

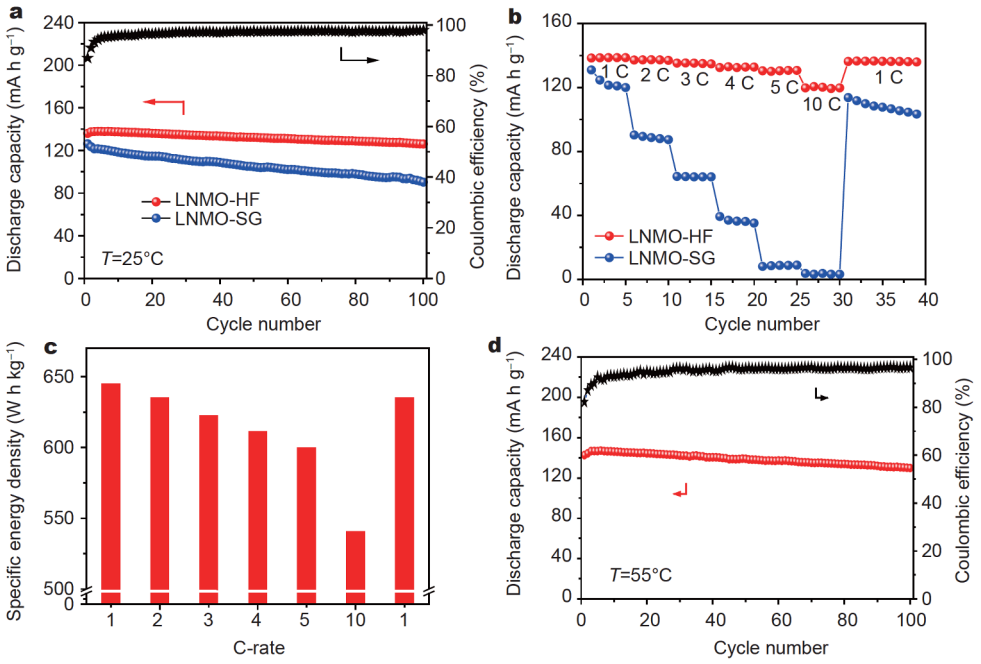

Figure 5 Galvanostatic charge/discharge and corresponding Coulombic efficiency at 1 C (1 C=147 mA h g^{-1}) at room temperature (a), rate performance from 1 to 10 C of LNMO-HF and LNMO-SG (b), specific energy density at various rates (c) and galvanostatic charge/discharge and corresponding Coulombic efficiency at 1 C at 55°C of LNMO-HF cathode (d).

sities. When the current densities increase from 1 to 10 C, the specific energy density slightly reduces from 644.6 to 540.4 W h kg^{-1}. Then the current rate was switched to 1 C and the obtained LNMO-HF cathode can deliver a specific energy density of 634.7 W h kg^{-1}. The corresponding discharge voltage plotted at various rates are presented in Fig. S5b. Furthermore, temperature is a main factor used to measure the cycle performance of spinel manganese-based cathode materials. When measured at 1 C under elevated temperature as shown in Fig. 5d, the LNMO-HF cathode yields an initial discharge capacity of 142.6 mA h g^{-1} almost equivalent to its theoretical specific capacity. The specific energy density was calculated to be 660.4 W h kg^{-1}. Even after 100 cycles, the capacity retention rate remains a high level of 91% with an efficiency of 96%. As a result, LNMO-HF cathode has high energy density, which can meet the demand of high specific energy density of EVs. Obviously, the resulting spinel LNMO-HF cathode improves the reversible lithium storage and shows outstanding cycling performance and rate capacity, which may be attributed to both 2D nanosheets and hierarchical flower-like microspheres. 2D nanosheets can facilitate the electron/Li^+ diffusion to enhance the electrochemical kinetics, and the hierarchical flower-like microspheres can effectively suppress the mechanical stress caused by Li^+ insertion/extraction during repeated cycling processes.

In order to better evaluate the cycling performance of the spinel manganese-based oxide nanosheet cathode, galvanostatic charge-discharge cyclic test at a high rate was conducted as shown in Fig. 6. The as-prepared LNMO-HF cathode has excellent cyclic stability and high reversible lithium storage at 10 C. The LNMO-HF delivers an initial discharge capacity of 122.0 mA h g^{-1} with the capacity retention of about 92.29% over 300 charge-discharge cycles and an efficiency of almost 100%. Up to 500 cycles, the capacity retention yields 83.68%. The high specific capacity and excellent cycle performance of high current densities further confirm the advantages of the hierarchical flower-like microspheres self-assembled by 2D nanosheets. The proposed Li^+/e^- transfer mechanism of the LNMO-HF cathode is illustrated in Fig. 6b. The unique structure can not only expose the maximized active sites and guaranty shortened ion/electron diffusion channels, but also effectively suppress the mechanical stress induced by Li^+ ions insertion/extraction during repeated cycling processes.

In addition, the galvanostatic charge/discharge profiles of LMO obtained by the same template-orientated strategy further confirm the advantages of hierarchical flower-

 © Science China Press and Springer-Verlag GmbH Germany, part of Springer Nature 2019

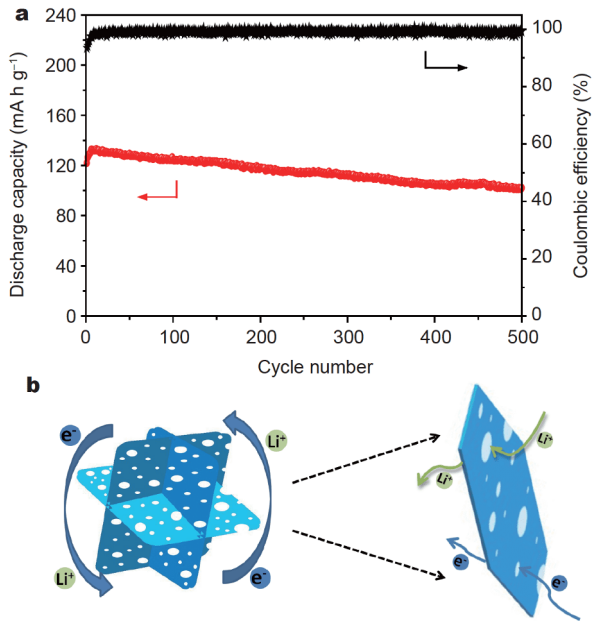

Figure 6 The galvanostatic cycling performance and corresponding Coulombic efficiency at 10 C (a) and the proposed e^-/Li^+ transfer mechanism (b) of LNMO-HF cathode.

like microspheres self-assembled by 2D nanosheets. The cycle performances of the spinel LMO cathode were carried at 5 C under room temperature and elevated temperature, respectively. As shown in Fig. 7a, b, the capacity retention of LMO are 100% and 92.45% after 100 cycles, respectively. Furthermore, the synthesized LMO was charged-discharged at various rates in Fig. 7c, exhibiting excellent rate performance. When the current density was switched to 1 C again, the discharge capacity still can recover to the initial discharge capacity. As shown in Fig. 7d, the LMO still yields capacity retention of 88.12% after 1000 cycles with the first discharge capacity of 113.7 mA h g^{-1} at high current density of 10 C.

CONCLUSIONS

The hierarchical flower-like spinel manganese-based oxide nanosheets cathode material was synthesized *via* a template-orientated strategy, where the employed template was fabricated by decomposition of carbonate obtained from "bubble reaction" with alcohol-assisted hydrothermal process. Compared with the LNMO-SG, the as-synthesized high-voltage LNMO-HF presents an

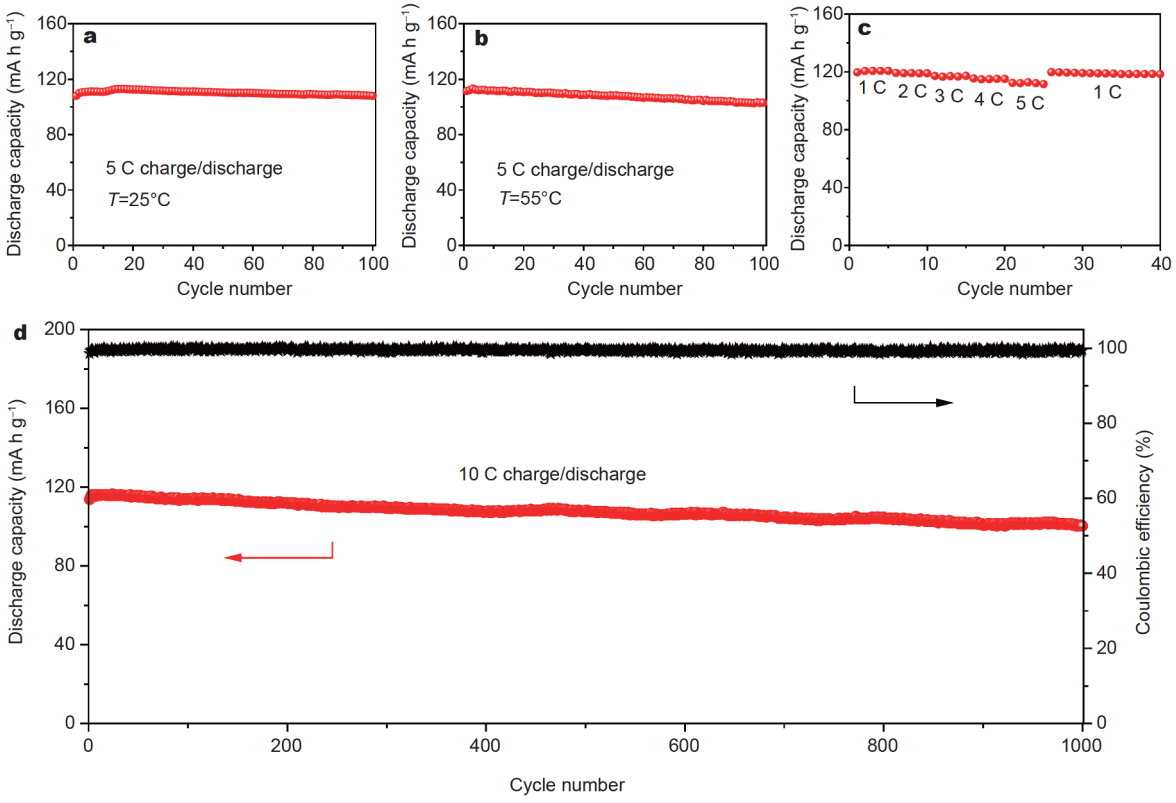

Figure 7 Galvanostatic charge/discharge at 5 C (1 C=148 mA h g^{-1}) at 25°C and 55°C (a and b), rate performance from 1 to 5 C (c), galvanostatic cycling performance test and corresponding Coulombic efficiency at 10 C (d) of the LMO cathode.

© Science China Press and Springer-Verlag GmbH Germany, part of Springer Nature 2019

initial capacity of 138.5 mA h g^{-1} at 1 C and achieves high capacity retentions of 94.2% at 5 C and 86.5% at 10 C. Furthermore, the LNMO-HF could also yield high discharge capacity of 142.6 mA h g^{-1} corresponding to high specific energy density of 660.7 W h kg^{-1} at 1 C under 55°C. Surprisingly, the template-orientated strategy was extended to LMO, which also achieved capacity retention of 88.12% after 1000 cycles. Thus good cycling stability, excellent rate capacity, as well as better elevated temperature performances of the resultant spinel manganese-based cathode material simultaneously well met the developing demand of high energy density. The high performance was attributed to the hierarchical microspheres self-assembled by 2D nanosheets, where the unique structure not only could expose the maximized active sites and shorten ion/electron diffusion channels, but also benefits structural stability and inhibits the structural strains induced by repeated cycling process.

Received 25 March 2019; accepted 17 May 2019; published online 12 June 2019

1 Crabtree G. The energy-storage revolution. Nature, 2015, 526: S92
2 Shi JL, Xiao DD, Ge M, *et al.* High-capacity cathode material with high voltage for Li-ion batteries. Adv Mater, 2018, 30: 1705575
3 Lee J, Kitchaev DA, Kwon DH, *et al.* Reversible Mn^{2+}/Mn^{4+} double redox in lithium-excess cathode materials. Nature, 2018, 556: 185–190
4 Hao J, Liu H, Ji Y, *et al.* Synthesis and electrochemical performance of Sn-doped $LiNi_{0.5}Mn_{1.5}O_4$ cathode material for high-voltage lithium-ion batteries. Sci China Mater, 2017, 60: 315–323
5 Manthiram A, Chemelewski K, Lee ES. A perspective on the high-voltage $LiMn_{1.5}Ni_{0.5}O_4$ spinel cathode for lithium-ion batteries. Energy Environ Sci, 2014, 7: 1339
6 Xiao J, Chen X, Sushko PV, *et al.* High-performance $LiNi_{0.5}Mn_{1.5}O_4$ spinel controlled by Mn^{3+} concentration and site disorder. Adv Mater, 2012, 24: 2109–2116
7 Zhang X, Cheng F, Yang J, *et al.* $LiNi_{0.5}Mn_{1.5}O_4$ porous nanorods as high-rate and long-life cathodes for Li-ion batteries. Nano Lett, 2013, 13: 2822–2825
8 Yin C, Zhou H, Yang Z, *et al.* Synthesis and electrochemical properties of $LiNi_{0.5}Mn_{1.5}O_4$ for Li-ion batteries by the metal-organic framework method. ACS Appl Mater Interfaces, 2018, 10: 13625–13634
9 Zhou L, Zhao D, Lou XWD. $LiNi_{0.5}Mn_{1.5}O_4$ hollow structures as high-performance cathodes for lithium-ion batteries. Angew Chem Int Ed, 2012, 51: 239–241
10 Wang J, Nie P, Xu G, *et al.* High-voltage $LiNi_{0.45}Cr_{0.1}Mn_{1.45}O_4$ cathode with superlong cycle performance for wide temperature lithium-ion batteries. Adv Funct Mater, 2018, 28: 1704808
11 Wu Y, Zhang J, Cao C, *et al.* $LiNi_{0.5}Mn_{1.5}O_4$ nano-submicro cubes as high-performance 5 V cathode materials for lithium-ion batteries. Electrochim Acta, 2017, 230: 293–298
12 Lian F, Zhang F, Yang L, *et al.* Constructing a heterostructural $LiNi_{0.4}Mn_{1.6}O_{4-\delta}$ material from concentration-gradient framework to significantly improve its cycling performance. ACS Appl Mater Interfaces, 2017, 9: 15822–15829
13 Zhu C, Mu X, van Aken PA, *et al.* Fast Li storage in MoS_2-graphene-carbon nanotube nanocomposites: Advantageous functional integration of 0D, 1D, and 2D nanostructures. Adv Energy Mater, 2015, 5: 1401170
14 Duan J, Chen S, Chambers BA, *et al.* 3D WS_2 nanolayers@heteroatom-doped graphene films as hydrogen evolution catalyst electrodes. Adv Mater, 2015, 27: 4234–4241
15 Wang Z, Rafai S, Qiao C, *et al.* Microwave-assisted synthesis of CuS hierarchical nanosheets as the cathode material for high-capacity rechargeable magnesium batteries. ACS Appl Mater Interfaces, 2019, 11: 7046–7054
16 Rui X, Zhao X, Lu Z, *et al.* Olivine-type nanosheets for lithium ion battery cathodes. ACS Nano, 2013, 7: 5637–5646
17 Chen L, Jiang H, Hu Y, *et al. In-situ* growth of ultrathin MoS_2 nanosheets on sponge-like carbon nanospheres for lithium-ion batteries. Sci China Mater, 2018, 61: 1049–1056
18 Zhao L, Dong B, Li S, *et al.* Interdiffusion reaction-assisted hybridization of two-dimensional metal–organic frameworks and $Ti_3C_2T_x$ nanosheets for electrocatalytic oxygen evolution. ACS Nano, 2017, 11: 5800–5807
19 Zhu Y, Cao T, Li Z, *et al.* Two-dimensional SnO_2/graphene heterostructures for highly reversible electrochemical lithium storage. Sci China Mater, 2018, 61: 1527–1535
20 Chen D, Peng L, Yuan Y, *et al.* Two-dimensional holey Co_3O_4 nanosheets for high-rate alkali-ion batteries: From rational synthesis to *in situ* probing. Nano Lett, 2017, 17: 3907–3913
21 Zhu Y, Cao C. A simple synthesis of two-dimensional ultrathin nickel cobaltite nanosheets for electrochemical lithium storage. Electrochim Acta, 2015, 176: 141–148
22 Wang W, Li P, Zheng H, *et al.* Ultrathin layered SnSe nanoplates for low voltage, high-rate, and long-life alkali-ion batteries. Small, 2017, 13: 1702228
23 Zhu Y, Cao T, Cao C, *et al.* A general synthetic strategy to monolayer graphene. Nano Res, 2018, 11: 3088–3095
24 Wang C, Li S, Han Y, *et al.* Assembly of $LiMnPO_4$ nanoplates into microclusters as a high-performance cathode in lithium-ion batteries. ACS Appl Mater Interfaces, 2017, 9: 27618–27624
25 Zhao Y, Peng L, Liu B, *et al.* Single-crystalline $LiFePO_4$ nanosheets for high-rate Li-ion batteries. Nano Lett, 2014, 14: 2849–2853
26 Peng L, Zhu Y, Khakoo U, *et al.* Self-assembled $LiNi_{1/3}Co_{1/3}Mn_{1/3}O_2$ nanosheet cathodes with tunable rate capability. Nano Energy, 2015, 17: 36–42
27 Tai Z, Subramaniyam CM, Chou SL, *et al.* Few atomic layered lithium cathode materials to achieve ultrahigh rate capability in lithium-ion batteries. Adv Mater, 2017, 29: 1700605
28 Zheng H, Chen X, Yang Y, *et al.* Self-assembled $LiNi_{1/3}Co_{1/3}Mn_{1/3}O_2$ nanosheet cathode with high electrochemical performance. ACS Appl Mater Interfaces, 2017, 9: 39560–39568
29 Wu Y, Cao T, Wang R, *et al.* A general strategy for the synthesis of two-dimensional holey nanosheets as cathodes for superior energy storage. J Mater Chem A, 2018, 6: 8374–8381
30 Xu M, Fei L, Zhang W, *et al.* Tailoring anisotropic Li-ion transport tunnels on orthogonally arranged Li-rich layered oxide nanoplates toward high-performance Li-ion batteries. Nano Lett, 2017, 17: 1670–1677
31 Wu Y, Cao C, Zhu Y, *et al.* Cube-shaped hierarchical $LiNi_{1/3}Co_{1/3}Mn_{1/3}O_2$ with enhanced growth of nanocrystal planes as high-performance cathode materials for lithium-ion batteries. J Mater Chem A, 2015, 3: 15523–15528

 © Science China Press and Springer-Verlag GmbH Germany, part of Springer Nature 2019

32 Wu Y, Cao C, Zhang J, *et al.* Hierarchical $LiMn_2O_4$ hollow cubes with exposed {111} planes as high-power cathodes for lithium-ion batteries. ACS Appl Mater Interfaces, 2016, 8: 19567–19572

33 Fan SS, Zhong H, Yu HT, *et al.* Hollow and hierarchical $Na_2Li_2Ti_6O_{14}$ microspheres with high electrochemical performance as anode material for lithium-ion battery. Sci China Mater, 2017, 60: 427–437

34 Huang ZD, Zhang TT, Lu H, *et al.* Bimetal-organic-framework derived $CoTiO_3$ mesoporous micro-prisms anode for superior stable power sodium ion batteries. Sci China Mater, 2018, 61: 1057–1066

35 Zhao Q, Wu Y, Ma X, *et al.* Mn oxidation state controllable spinel manganese-based intergrown cathode for excellent reversible lithium storage. J Power Sources, 2017, 359: 295–302

36 Li M, Yang W, Huang Y, *et al.* Hierarchical mesoporous Co_3O_4@$ZnCo_2O_4$ hybrid nanowire arrays supported on Ni foam for high-performance asymmetric supercapacitors. Sci China Mater, 2018, 61: 1167–1176

37 Hou J, Cao C, Idrees F, *et al.* Hierarchical porous nitrogen-doped carbon nanosheets derived from silk for ultrahigh-capacity battery anodes and supercapacitors. ACS Nano, 2015, 9: 2556–2564

38 Yang S, Chen J, Liu Y, *et al.* Preparing $LiNi_{0.5}Mn_{1.5}O_4$ nanoplates with superior properties in lithium-ion batteries using bimetal-organic coordination-polymers as precursors. J Mater Chem A, 2014, 2: 9322–9330

Acknowledgements This work was financially supported by the National Natural Science Foundation of China (21371023).

Author contributions Cao C conceived the strategy. Zhao Q performed the experiments with support from Guo Z, Wu Y, Wang L, Han Z, Ma X, and Zhu Y. All authors contributed to the general discussion.

Conflict of interest The authors declare no conflict of interest.

Supplementary information Supporting data are available in the online version of the paper.

Chuanbao Cao is currently the chief responsible professor of the School of Materials Science and Engineering, Director of Research Center of Materials Science of Beijing Institute of Technology, China. His research is focused on the electrochemical energy storage and conversion including electrode materials of lithium ion battery, supercapacitors, catalyst and photo-electrochemical materials. Until now, he has published more than 320 peer-review research papers, holds or has filed 50 patents and patent applications.

多级花状尖晶石锰基氧化物纳米片用于高性能锂离子电池

赵全清[1], 郭泽峰[2], 吴宇[1], 王利芹[1], 韩占立[1], 马西兰[1], 朱有启[1], 曹传宝[1*]

摘要 由二维(2D)纳米片组装成的多级花状结构有利于电化学反应. 这种独特的结构不仅可以暴露更多的活性位点、 缩短离子/电子扩散路径, 还可以确保良好的结构稳定性, 抑制重复循环过程中的结构应变. 本文通过模板导向策略合成多级花状纯相尖晶石锰基氧化物纳米片. 通过醇辅助水热法, 利用“气泡反应”原理获得的碳酸盐分解来制备取向模板. 最终产物尖晶石锰基氧化物纳米片同时满足优异的倍率性能和循环稳定性要求. 合成的分层花状高压$LiNi_{0.5}Mn_{1.5}O_4$ (LNMO-HF)元素分布均匀, 且无杂相. LNMO-HF可以提供142.6 mA h g^{-1}的高放电容量, 在55°C、1 C下, 其比能量密度为660.7 W h kg^{-1}. 此外, 利用这种模板导向策略合成的$LiMn_2O_4$ (LMO), 在1000次循环后, 其容量保持率可达88.12%.

 © Science China Press and Springer-Verlag GmbH Germany, part of Springer Nature 2019